A Critical Review of Rail Track Geotechnologies Considering Increased Speeds and Axle Loads

Buddhima Indraratna[1], Sanjay Nimbalkar[2] and Cholachat Rujikiatkamjorn[3]
[1]*Professor of Civil Engineering and Research Director, Centre for Geomechanics and Railway Engineering, University of Wollongong, Australia*
[2]*Research Fellow, Centre for Geomechanics and Railway Engineering, University of Wollongong, Australia*
[3]*Associate Professor, School of Civil, Mining and Environmental Engineering, University of Wollongong, Australia*
E-mail: indra@uow.edu.au

ABSTRACT: Ballasted railroads are designed to provide high speed commuter and heavy haul transportation. Ballast is one of most important load bearing components of the track substructure. However, it often experiences excessive settlement, lateral deformation and particle breakage when subjected to large dynamic (cyclic and impact) stresses. In addition, tracks constructed along coastal areas often undergo large settlements over soft compressible estuarine deposits, leading to frequent and costly track maintenance. The use of artificial inclusions such as geogrids, geocomposites, shock-mats (rubber) and prefabricated vertical drains (PVDs) are attractive options to maintain the vertical and horizontal alignment of tracks and to curtail excessive maintenance costs. This critical review paper provides a deeper insight to the recent advancements in rail track geotechnology at increased train speeds and axle loads.

KEYWORDS: Ballasted railroads, Cyclic loads, Particle breakage, Geosynthetics, Prefabricated vertical drains

1. INTRODUCTION

Ballasted rail tracks offer one of the largest transportation networks in the world. However they are very maintenance intensive, as the granular substructure layers (ballast, capping and structural-fill) often undergo significant deformations due to high cyclic stresses exerted by increasingly heavier and faster trains. These problems become more severe when tracks are constructed over hard rock terrains or on concrete bridge decks where large dynamic (impact) loads are sustained. These cyclic and impact loads also cause rapid fragmentation of ballast aggregates and the subsequent clogging of ballast voids due to intrusion of fines such as clay and coal (Selig and Waters 1994; Indraratna et al. 2014a, Indraratna et al. 2012b, Ngo et al. 2014, Tennakoon et al. 2015), apart from the fines from the crushed ballast. The confining pressure is a key parameter controlling the stability of ballasted tracks (Lackenby *et al*. 2007, Indraratna et al. 2014b,c). Ballast breakage can be categorized into three distinct zones, namely, the dilatant unstable degradation zone, the optimum degradation zone, and the compressive stable degradation zone according to the level of prevailing confining pressure (Indraratna et al. 2005a). The permanent deformation and breakage of ballast are also found to be affected by the magnitude of wheel load (= axle load/2), train speed (frequency) (Sun et al. 2014; 2015) and impact loads (Indraratna et al. 2014d), which depend on the type and nature of irregularities in the wheels or rails, as well as on the dynamic track response (Jenkins et al. 1974, Auersch 2006, Indraratna et al. 2014e).

Among several ground improvement techniques available, using geosynthetic products such as geogrid, geotextile or geocomposite (bonding geogrid with geotextile) have drawn more attention, owing to their economical and relatively swift installation. The potential use of geogrid and geocomposite in the enhancement of track stability is demonstrated elsewhere (Raymond 2002, Indraratna and Salim 2003, Indraratna *et al*. 2007, 2010a, Indraratna and Nimbalkar 2013, Indraratna et al. 2015). Installing resilient mats such as shock-mats (rubber sheets) in rail tracks can greatly assist in attenuation of impact-induced stresses (Nimbalkar et al. 2012). Until today, only very limited field studies have been reported which quantify the relative performance of geosynthetics and shock mats in tandem (Indraratna *et al*. 2010a, 2013a, 2014c,e).

Large scale laboratory testing in combination with full-scale instrumented field studies often represent an efficient strategy for accurately assessing track degradation. In this regard, extensive field trials on sections of an instrumented track at Singleton in the state of New South Wales, Australia have been conducted. The details of field instrumentation and monitoring processes along with the findings of this unique field study are discussed herein.

The behavior of saturated clays (subgrade) subjected to cyclic loading is of significant importance in the design of railroads. Soft clays (estuarine or marine) located along coastline in Australia have undesirable geotechnical properties such as low bearing capacity and high compressibility. Excessive settlement and lateral movement adversely affect the stability of port and transport infrastructure including rail embankments built on such soft compressible ground (Indraratna and Redana 2000; Bergado *et al*. 2002; Indraratna *et al*. 2009, 2011). To enable the construction of rail embankments over soft clay terrains, adequate effort in ground improvement such as the use of prefabricated vertical drains (PVDs) is required to eliminate excessive settlement and lateral movement (Indraratna et al. 2008; Indraratna et al. 2010b; Indraratna et al. 2012a). In shallow depths of subgrade, relatively short PVDs can help to dissipate cyclic load induced pore water pressures, limit horizontal movements and increase the bearing capacity of the soft subgrade, and these aspects need to be properly analysed under *in-situ* track conditions. This paper describes the results of these two unique full-scale field trials plus a series of large-scale laboratory tests supplemented by finite element analyses to assess the performance of ballasted tracks at increased speeds and axle loads, and to quantify the benefits of using synthetic inclusions in track.

2. INFLUENCE OF TRAIN SPEED (FREQUENCY)

The influence of train speed on the permanent deformation and degradation of ballast during cyclic loading was studied using the large scale triaxial apparatus designed and built at the University of Wollongong as shown in Figure 1. The grain size distribution of ballast specimens was prepared in accordance with the current industry practices in Australia [AS 2758.7, 1996].

2.1 Laboratory Testing

Latite basalt, a commonly used ballast aggregates in Sydney suburbs, was used in this study (Los Angeles abrasion <25%, Flakiness index <30%). It was thoroughly cleaned, dried, and compacted in four layers to a density of about 1510 kg/m^3 to simulate the typical field density in heavy haul railroads. These specimens were then isotropically consolidated to a confining pressure (σ'_3) of 10, 30 and 60 kPa. A wide range of frequencies varying from 5 Hz to 60 Hz was selected to simulate train speeds from about 40 to 400 km/h. The maximum cyclic deviator stress ($q_{max,cyc}$) of 230 and 370 kPa was used to represent axle loads of 25 and 40 tonnes, respectively. Cyclic tests were conducted up to 500,000 load cycles or until vertical deformation had reached the limit of the equipment (@ 30% axial strain).

(a) (b)

Figure 1 (a) Large-scale tri-axial rig; (b) test specimen (Indraratna et al. 2009, with permission from ASCE)

2.2 Test Results

Figure 2 presents the variation of axial strain (ε_a) with the number of cycles (N) for different frequencies (f) and amplitudes ($q_{max,cyc}$) of cyclic loading. A significant increase in ε_a with f was observed. For a particular value of f, ε_a rapidly increased to maximum value (e.g, 30 % at $N = 2 \times 10^4$ for $f = 40$ Hz). At other frequency levels, ε_a rapidly increased during the initial cycles, after which a permanent ε_a attained a stable value at large N. This sudden increase in ε_a at low values of N could be attributed to the particle re-arrangement and corner breakage. In addition, it was evident that with an increase in f, higher values of N are required to stabilise ε_a to a steady level.

Sun et al (2014) highlighted the existence of four regimes of permanent deformations based on the applied cyclic loads: (a) the zone of elastic shakedown exhibited by no plastic strain accumulation, (b) the zone of plastic shakedown characterised by a steady-state response with a small accumulation of plastic strain, (c) a ratcheting zone that shows a constant accumulation of plastic strain and (d) a plastic collapse zone where the plastic strains accumulate rapidly and failure occurs in a relatively short time. In this study, three different deformation mechanisms were observed in response to frequency of loading, namely, in Range I: plastic shakedown at $f \leq 20$ Hz, in Range II: plastic shakedown and ratcheting at 30 Hz $\leq f \leq$ 50 Hz, and in Range III: plastic collapse at $f \geq 60$ Hz.

In summary, a critical frequency can be identified above which the risk of track failure is imminent. As shown in Figure 2, the critical frequency range is 20-40 Hz depending on level of confinement (σ'_3). The influence of frequency (f) and maximum cyclic deviator stress ($q_{max,cyc}$) on ballast breakage is shown in Figure 3. Ballast breakage is measured using BBI proposed by Indraratna et al. (2005a) for different values of f and $q_{max,cyc}$. It is seen that the load frequency (f) has a profound influence on the magnitude of BBI, which increased with f. For the tested ballast (latite basalt), distinct ballast degradation behaviors were observed corresponding to different deformation ranges during cyclic testing.

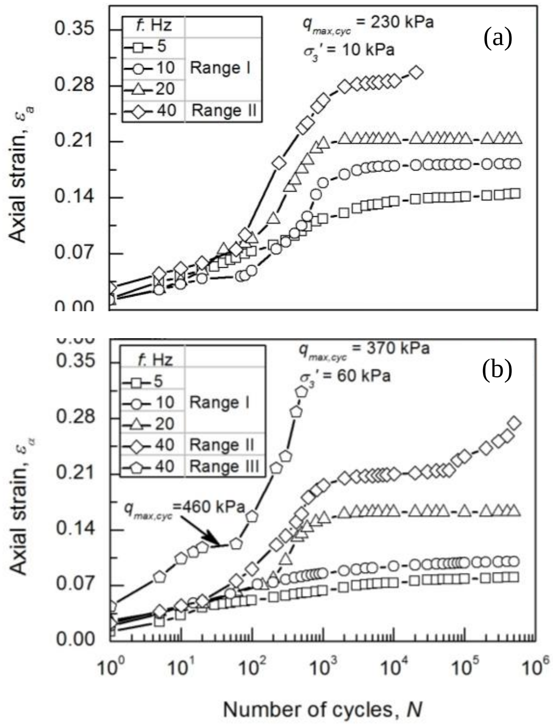

Figure 2 Variation of axial strain (ε_a) versus number of cycles (N) (Sun et al. 2015, with permission from ASCE)

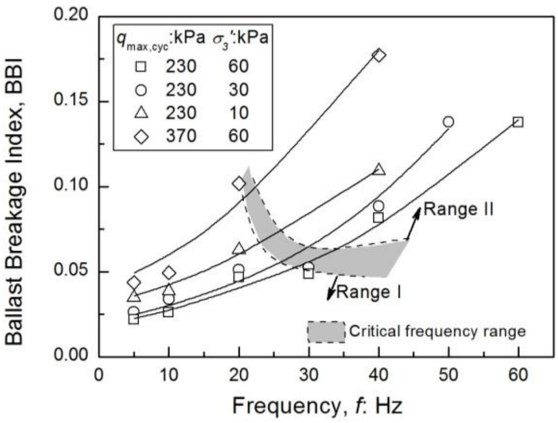

Figure 3 Variation of ballast breakage index (BBI) with various frequencies (f) (Sun et al. 2015, with permission from ASCE)

For Range I ($f \leq 30$ Hz), the particle degradation was in the form of attrition of asperities and corner breakage as shown in Figure 4(a). As the frequency became higher ($30 < f < 60$ Hz) in Range II, a high degree of attrition resulting from increased vibration became predominant (Figures 4(b) and 4(c)). At very high frequency ($f \geq 60$ Hz) in Range III, the coordination number is greatly reduced, which would induce particle splitting as shown in Figure 4(d). Figure 3 shows that the critical frequency decreases as the particle breakage increases. Ratcheting failure (Range III) of the specimen would occur with a significant particle breakage (BBI > 0.10) even at a relatively low value of frequency (i.e., $f = 25$ Hz).

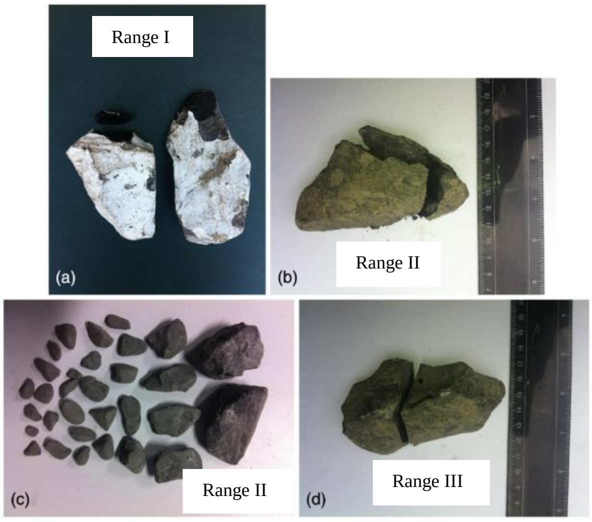

Figure 4 Examples of ballast degradation: (a) corner breakage; (b) particle splitting; (c) high degree attrition of asperities; (d) particle splitting (Sun et al. 2015, with permission from ASCE)

3. INFLUENCE OF IMPACT FORCES AND BENEFITS OF USING SHOCK MATS

The impact forces occur due to imperfections in the wheels or rails such as flat wheels, rail corrugation, dipped weld joints. These irregularities are distinct in nature and can cause the train wheels to impose impact forces on the rail (Bian et al., 2013; Indraratna et al., 2014d). At a bridge approach, road crossing or track transition zone where the foundations stiffness changes from ballasted to slab track or vice versa, high impact forces are generated, usually resulting in track degradation (Li and Davis, 2005).

Two types of force peaks (P_1 and P_2) are normally observed during impact loading. The impact force P_1 is due to the inertia of the rail and sleepers resisting the downward motion of the wheel. It is often characterized by an instantaneous sharp peak. The force P_2, lesser in magnitude compared to P_1, prevails over a longer duration. The force P_2 mainly affects the track substructure leading to its significant compression (Frederick and Round, 1985). Jenkins et al. (1974) proposed a simplified empirical formula to calculate P_2 (unit in kN) forces:

$$P_2 = P_0 + 2\alpha V_m \times \sqrt{\frac{M_u}{M_u + M_t}} \times \left[1 - \frac{C_t \pi}{4 \times \sqrt{K_t (M_u + M_t)}}\right] \times \sqrt{K_t M_u} \tag{1}$$

where, P_0 is maximum static wheel load (kN), M_u is vehicle unsprung mass per wheel (kg), 2α is total dip angle (radians), V_m is maximum normal operating velocity (m/s), M_t is an equivalent vertical rail mass per wheel (kg), K_t is an equivalent vertical rail stiffness per wheel (MN/m) and C_t is an equivalent vertical rail damping per wheel (kNs/m).

In order to evaluate effects of impact forces on ballast deformation and degradation, a series of laboratory tests were carried out using a large scale drop-weight impact testing equipment as shown in Figure 5. The effectiveness of shock mats in the attenuation of high frequency impact loads was also investigated. A thin layer of compacted sand was used to simulate a typical 'weak' subgrade. In this study, a 10 mm thick shock mat used in the study was made of recycled rubber granulates of 1-3 mm size particles, bound by a polyurethane elastomer compound (tensile strength = 600 kN/m^2, tensile strain at failure = 80%, Modulus at 10% compressive strain = 3800 kN/m^2).

Figure 5 Drop weight impact testing equipment

3.1 Laboratory Testing

The ballast was thoroughly cleaned, dried, sieved through a set of standard sieves (aperture size ranging from 53 mm to 13.2 mm). The ballast specimens (C_u = 1.6, C_c = 1.0, and d_{50} = 35 mm) were compacted in several layers to simulate the field densities of heavy haul tracks. In order to resemble low track confining pressure in the field, test specimens were confined in a rubber membrane. In this study, typical dynamic stresses in the range of 400-600 kPa caused by wheel flat and dipped rail (Steffens and Murray, 2005; Indraratna et al., 2010a) were simulated. The drop hammer was raised mechanically to the required height and then released by an electronic quick release system. The free fall drop hammer has a weight of 592 kg and it can be dropped from a maximum height of 6 m. The free fall hammer velocity efficiency is 98% due to the friction of the guiding column (Kaewunruen and Remennikov, 2010). Considering this, the actual drop height (h_a) was calculated using the following equation:

$$h_a = \frac{(V/0.98)^2}{2g} \tag{2}$$

where, V is hammer velocity. The impact force caused by hammer was measured by a dynamic load cell of a capacity of 1,200 kN mounted at the bottom of the hammer. The impact load was stopped after 10 blows due to an attenuation of strains in the ballast layer.

3.2 Experimental Observations

As discussed in previous section, as P_2 forces mainly influence ballast and subgrade, they were plotted against number of blows as shown in Figure 6. P_2 force shows a gradual increase with the increased number of blows. This is because the ballast develops a denser packing assembly due to reorientation and rearrangement of ballast aggregates. A dense aggregate matrix offers a higher inertial resistance which leads to an increased value of P_2. A rapid increase of P_2 occurs at the lower number of blows (i.e. $N \leq 4$), but becomes almost insignificant after the eighth blow. This indicates that the ballast layer attains stabilization after a certain number of impacts to produce an almost constant P_2. Even without a shock mat, a ballast bed placed on a weak subgrade leads to a decreased magnitude of impact force compared to a stiffer subgrade.

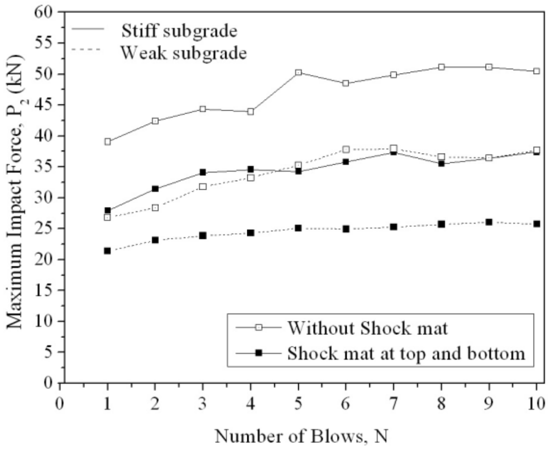

Figure 6 Variation of impact force with number of blows (data sourced from Nimbalkar et al. 2012)

Particle degradation adversely affects the strength and deformation of ballast (Selig and Waters 1994, Indraratna et al. 2005a). After each test, a bulk sample of ballast was sieved to obtain the *BBI*, the values of which are presented in Table 1. The higher ballast breakage can be attributed to the considerable non-uniform stress concentrations occurring at the corners of the sharp angular aggregates. It was noticed that the breakdown of ballast materials consistent with other laboratory durability tests (i.e. Los Angeles abrasion). The application of just 10 impact blows caused considerable ballast breakage (i.e. *BBI* = 17%) when a stiff subgrade was used, but when a shock mat was placed at two locations (i.e. above and below the ballast layer), the breakage was reduced by approximately 47% for a stiff subgrade and about 65% for a relatively weak subgrade.

Table 1 Ballast breakage under impact loading (Indraratna *et al*. 2014c)

Test No.	**Base type**	**Placement Details of Shock Mats**	***BBI***
1	Stiff	Without shock mat	0.170
2	Stiff	Shock mat at top and bottom	0.091
3	Weak	Without shock mat	0.080
4	Weak	Shock mat at top and bottom	0.028

4. EFFECTS OF CYCLIC LOADS ON LATERAL STABILITY OF BALLASTED TRACK AND USE OF GEOGRIDS

A series of drained triaxial tests were conducted using the Process Simulation Prismoidal Triaxial Apparatus (PSPTA) as shown in Figure 7a. This large-scale apparatus is 800 mm in length, 600 mm in width and 600 mm in height. It is large enough to accommodate a unit cell size representing the effective sleeper length and the sleeper spacing (Indraratna et al. 2015). The effective sleeper length is assumed to be one-third of the total sleeper length (L = 2400 mm) and the sleeper spacing (s) is 600 mm. The modification involved the replacement of the side wall with a wall containing five movable plates each of 64 mm in height (Figure 7b), to represent a more realistic stress and strain distribution with depth.

4.1 Laboratory Testing

A dynamic vertical stress of 460 kPa corresponding to an axle load of 225 kN was applied onto the test specimen. A lateral confining pressure of 10 kPa was applied onto the side wall with five movable plates. While other three walls were held fixed, the modified side wall was allowed to move laterally. Cyclic tests were carried at a frequency of 20 Hz, which corresponds to a train speed of about 150 km/h. Tests were conducted up to 250,000 load cycles.

Figure 7(a) Process Simulation Prismoidal Triaxial Apparatus (PSPTA) designed and built at University of Wollongong

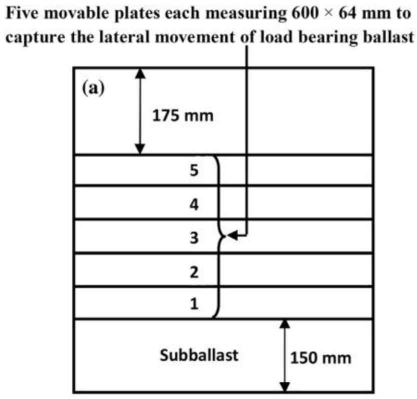

Figure 7(b) Schematic diagram of the side wall of the MPST apparatus (Indraratna et al. 2013b)

The geogrids were selected based on the interface efficiency factor (α), obtained from direct shear tests (Indraratna et al. 2013b). It was observed that the normalised aperture ratio (A/D_{50}, where A is aperture size and D_{50}, is median particle size) had a profound influence on the interface efficiency factor (α). The best size geogrid aperture to optimise the interface shear strength was $1.20D_{50}$. The minimum and maximum sized apertures required to attain the beneficial effects of geogrids were $0.95D_{50}$ and $2.50D_{50}$, respectively. In accordance, four types of biaxial geogrid were used in this study: geogrid 'G1' (aperture size, A = 38 × 38 mm), geogrid 'G2' with triangular aperture (A = 36 × 36 mm), geogrid 'G3' (A = 65 × 65 mm), and geogrid 'G4' (A = 44 × 42 mm). The physical characteristics and the technical specifications of the geogrids are discussed elsewhere (Indraratna et al. 2013b). The geogrid was placed at either z = 0 mm or z = 65 mm, where z is the distance above the subballast-ballast interface.

4.2 Interpretation of Test Data

The improved performance of geogrid-reinforced ballast can be evaluated in terms of a normalized parameter termed as Lateral Spread Reduction Index (*LSRI*). It is defined as (Indraratna et al. 2013b):

$$LSRI = \frac{S_{l(unreinforced)} - S_{l(reinforced)}}{S_{l(unreinforced)}} \tag{3}$$

where, $S_{l(unreinforced)}$ and $S_{l(reinforced)}$ are lateral deformations of unreinforced and geogrid-reinforced ballast, respectively. LSRI of zero indicates unreinforced condition whereas a value of unity represents no lateral spreading. On the other hand, a negative value of LSRI indicates an increase in lateral deformation due to the inclusion of reinforcement.

Figure 8 shows the variation of average LSRI along the depth with the ratio A/D_{50}, for both the geogrid placement positions (i.e. at z = 0 and 65 mm). The values of A/D_{50} for different geogrids were adapted from Indraratna et al. (2012a). For geogrid placed below ballast, the average LSRI increased significantly from 0.06 to 0.25 as A/D_{50} increased from 0.6 to 1.20. This may be attributed to the better geogrid-particle interlock attained as the geogrid aperture size increases for a given ballast size. The geogrid 'G4' with A/D_{50} of 1.21 resulted into a maximum LSRI of 0.25. However, with the further increase in A/D_{50} from 1.21 to 1.85, the average LSRI decreased from 0.25 to 0.20. For the geogrid placed at 65 mm above the subballast, the average LSRI followed an almost similar trend with A/D_{50} except that the geogrid 'G2' exhibited a negative LSRI.

As the average LSRI increased, both the deformation and the particle breakage reduced significantly. The deformation and BBI decreased from about 23.5 to 9.8 mm and 9.89 to 4.6%, respectively, as the average LSRI increased from zero to 0.37. A linear increase in deformation was observed with the increase in BBI as given by (Indraratna et al. 2013b):

$$S_{v(reinforced)} = 0.0243BBI - 1.74 \tag{4}$$

As highlighted in Equation (4), the particle breakage also contributed to a significant portion of deformation.

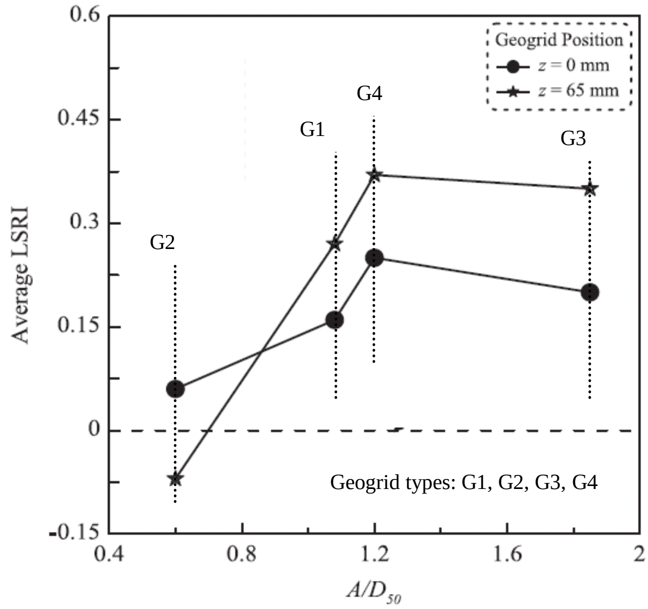

Figure 8 Variation of average LSRI with A/D_{50}
(data sourced from Indraratna et al. 2013b)

5. EFFECTS OF CYCLIC LOADS ON RADIAL DRAINAGE AND USE OF PVDS

Soft clays are extensively found in many coastal regions of Australia up to significant depths, including the coastal low lying areas of NSW. These soft clays can sustain high excess pore water pressure during static and repeated cyclic loading. The use of prefabricated vertical drains (PVDs) is one of the popular methods for improvement of such soft compressible ground. The effectiveness of PVDs for dissipating cyclic pore water pressures is discussed in this study. A large scale triaxial test apparatus was used to examine the effects of cyclic load on radial drainage and consolidation by PVDs (Figure 9).

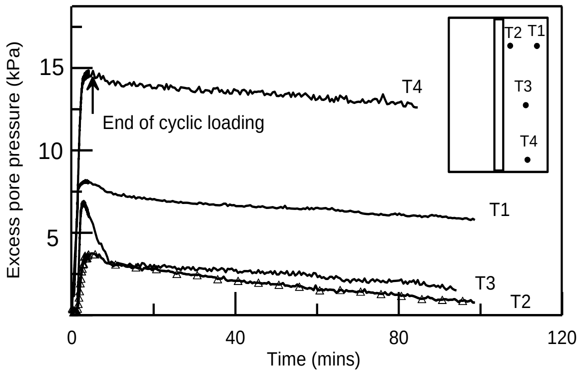

Figure 9 Dissipation of excess pore pressure at various locations from the PVD (Indraratna et al. 2009, with permission from ASCE)

5.1 Laboratory Procedure

The test specimen of reconstituted estuarine clay was lightly compacted to a unit weight of about 17 to 17.5 kN/m^3. The specimen was consolidated under k_0 conditions that may typically vary in many coastal regions of Australia from 0.6-0.7. Upon finishing the consolidation, the cyclic loading was applied at frequencies of 5-10 Hz, typically simulating train speeds of say 60-100 km/h with 25-30 tonnes/axle train loads.

5.2 Laboratory Results

The cyclic behaviour of saturated samples mainly depends on the build-up of pore water pressures and the associated reduction in effective stresses during cyclic loading. Figure 9 shows an example of the excess pore pressure recorded. This indicates that the maximum excess pore water pressure closer to the PVD (location T2) during cyclic load was significantly less than that near the cell boundary (location T1), and the dissipation rate of excess pore pressure at location T2 is faster than that of location T1.

Excess pore water pressure ratio (R_u) is defined as the excess pore water pressure normalized to the effective initial confining pressure. Figure 10 shows the excess pore pressures and corresponding excess pore water pressure ratio R_u versus the number of loading cycles N under the three separate series of tests. Without PVD, the excess pore pressure would increase rapidly $R_u \approx 0.9$, and undrained failure would occur very quickly.

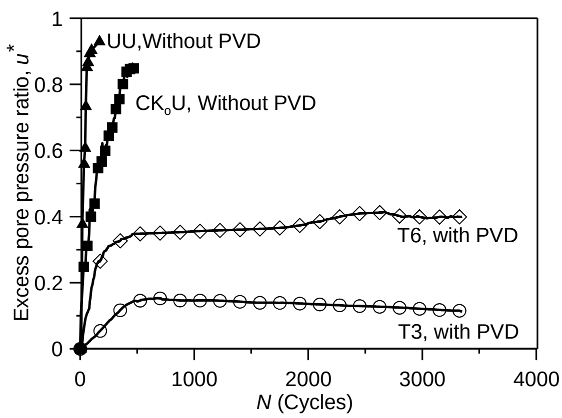

Figure 10 Excess pore pressure generated under cyclic loading (Indraratna et al. 2009, with permission from ASCE)

The corresponding axial strains are shown in Figure 11a. Without a PVD, large cyclic axial strains develop and failure occurs rapidly after about 200 cycles in the cyclic CK_0U test, and after about 100 cycles in the cyclic confined compression test. As seen from Figure 11b, failure is detected when ε_a-log$N$ curves begin to concave rapidly downwards. With a PVD, the axial strain gradually increases to a constant level and no failure is evident even after 3,000 cycles, as shown in Figs 11(a and b). The test results revealed that PVDs effectively decreased the maximum excess pore pressure, even under cyclic loading, and they also decreased the build- up of excess pore pressure and helped to accelerate its dissipation during any rest periods. In reality, dissipating pore water pressure during a rest period stabilises the track for the next loading stage (i.e. subsequent passage of train). This cyclic-induced excess pore pressure tends to rise substantially as the shear strain exceeds 1.5-2%. Soft clays provided with radial drainage via PVD can be subjected to cyclic stress levels higher than the critical cyclic stress ratio without causing undrained failure.

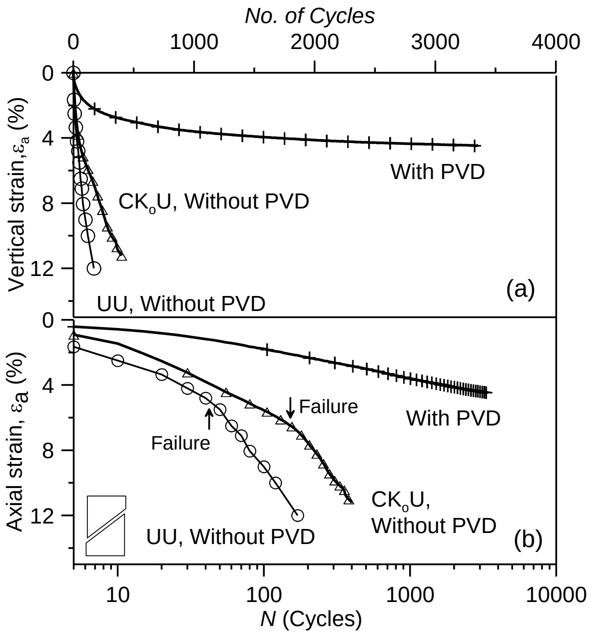

Figure 11 Axial strains during cyclic loading versus number of loading cycles (N): (a) arithmetic; (b) semi logarithmic scales (Indraratna et al. 2009, with permission from ASCE)

6. USE OF GEOSYNTHETICS AND SHOCK MATS FOR RAIL INFRASTRUCTURE: FIELD STUDY AT SINGLETON

To investigate how well different types of geosynthetics would improve the overall stability of the track under in situ conditions, an extensive study was undertaken on fully instrumented sections of track. Construction of the track was started in July 2009 and the track was commissioned in May 2010 and the location of the track is illustrated in Figure 12a. The sub-surface investigation indicated that the presence of a massive sedimentary outcrop of rock for some track part (chainage 224.2 to 229.0 km) while flood plain of the nearby Hunter River was located for remaining track part (Indraratna et al. 2013a). The flood plain consisted of a layer of an alluvial deposit of silty clay 7-10 m thick, underlain by heterogeneous layers of medium dense sand and silty clay.

6.1 Construction of Track

Eight experimental track sections were constructed on three different types of sub-grades, including (i) the relatively soft general fill and alluvial silty clay deposit (Sections 1-5 and Section A), (ii) the intermediate cut siltstone (Sections 6 and C), and (iii) the stiff reinforced concrete bridge deck supported by a piled abutment (Section B), as shown in Figure 12(a). The track substructure consisted of a 300 mm thick layer of ballast underlain by a 150 mm thick layer of sub-ballast. A structural layer of fill with a minimum of 500 mm thickness was placed below the sub-ballast.

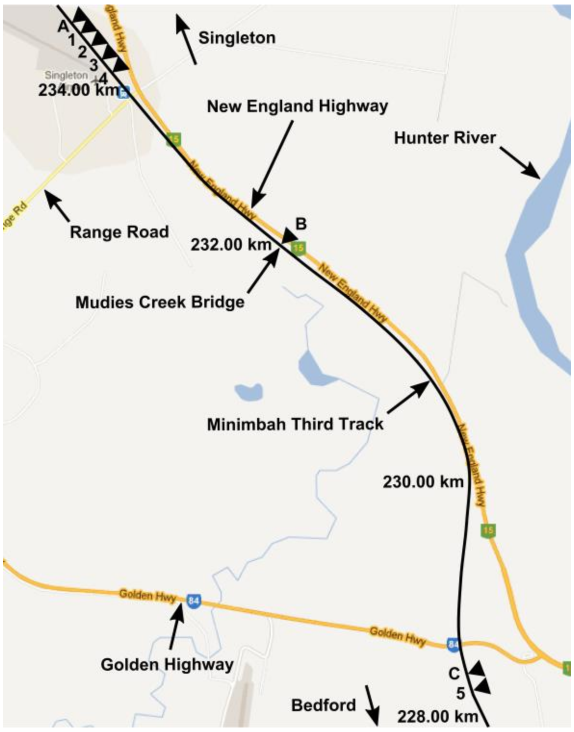

Figure 12(a) Locations of Minimbah Third Track sections with different values of subgrade stiffness

Three types of biaxial geogrid were used in this study: (i) geogrid 'G3' (A = 65 × 65 mm), (ii) geogrid 'G5' (aperture size, A = 44 × 44 mm), and (iii) geogrid 'G6' (A = 44 × 44 mm). A layer of geogrid was placed at Sections 1-3 and 5 while a layer of geocomposite (geogrid 'G7' with aperture size A = 31 × 31 mm combined with nonwoven geotextile) was placed at Section 4. The shock mat was made of recycled rubber granulates of 1-3 mm sizes encapsulated by a polyurethane elastomer compound. A layer of shock mat was placed at the Mudies Creek bridge in Singleton, NSW. Figure 12(b) shows the location of this bridge and the installation of shock mats. More details on physical characteristics and the technical specifications of the geosynthetic grids and shock mats are given elsewhere by Indraratna et al. (2014e).

Figure 12(b) Location of Mudies Creek Bridge and Installation of shock mat

6.2 Track Instrumentation

Figure 13 shows the placement details of instruments at the experimental sections of track. Strain gauges were used to study deformations and mobilised forces along the layers of geogrid (Figure 13a). Traffic induced stresses were monitored by pressure cells (Figure 13b). Transient deformations of the ballast were measured by deformation frame as shown in Figure 13c. Five potentiometers (POTs) were mounted on a custom built deformation frame. Settlement pegs were installed between the sleeper and ballast and between the ballast and sub-ballast to measure vertical deformations of the ballast (Figure 13d). Details of track sections are illustrated in Figure 13e.

All the field measurements were obtained from the aforementioned instruments using a computer controlled data acquisition system. A frequency of 2000 Hz was chosen to obtain transient records of stresses.

6.3 Track Measurements and Data Interpretation

The deformation of ballast was determined by subtracting the vertical displacement of the ballast-capping interface from that at the sleeper-ballast interface. The vertical deformation (S_v) of the ballast is plotted against number of load cycles (N) in Figures 14 and 15 for soft embankment and hard rock, respectively. These results indicate that the relationship between deformation and number of load cycles is non-linear, regardless of how the track was reinforced. The rate of increase of S_v diminished as the number of load cycles increased.

When the results for sections on similar subgrades were compared to each other, vertical settlements of the reinforced sections were 10-32% smaller than those without reinforcement. This pattern is similar to that observed in the laboratory (Brown et al. 2007), and it can be attributed mainly to the interlocking between ballast particles and geogrids. When the results for sections with similar geogrids are compared, it is apparent that the ability of geogrid reinforcement to reduce track deformation is generally greater for softer subgrades (low track stiffness). Moreover, geogrid 'G5' performed most effectively as its aperture size (40 mm) enabled better interlocking of the ballast particles. This finding also agrees with the criteria for optimum size apertures for reinforcing geogrids discussed in the preceding section. When Sections A, B, and C are compared, the results indicate that the vertical deformations are larger when the subgrade becomes weaker, i.e., S_v was smaller at section B and larger than section A.

Transient deformations of the ballast layer were measured by a custom made deformation frame. It was observed that the passage of train with an axial load of 30 tonnes travelling at 40 km/h resulted in a vertical deformation (S_{tv}) between 1.5 to 3.0 mm, resulting in an average vertical strain (ε_{tv}) of 0.5 - 1.0%. The transient lateral deformations of ballast (S_{th}) measured on the shoulder were all expansive and between -0.5 to -0.3 mm. This resulted in an average lateral strain (ε_{th}) of -0.05 to -0.02%. The lateral strains were larger near the crest and smaller near the toe of ballast. The average transient strains of track sections with reinforcement (i.e. Sections 1-3, 5) were about 15% smaller than those without reinforcement (i.e. Section A, C), regardless of the type of geosynthetics used.

The vertical stresses (σ_v) due to the passage of trains with an axle load of 30 tonnes travelling at about 40 km/h were about 280 kPa at Section B (mat-deck interface) and between 30 to 40 kPa at Sections 1, 6, A, and C (ballast-sub-ballast interface). Vertical stresses at the sleeper-ballast interface of the latter were between 170 to 190 kPa, which indicate that the traffic-induced stresses were considerably larger in the track having a stiffer subgrade.

As anticipated, the larger stresses also caused more breakage of individual particles of ballast. Particle breakage was quantified in terms of BBI and its values are given in Table 2. As expected, the ballast breakage was highest at the top of the layer, and reduced with depth. Largest values of BBI obtained at hard rock verified that particle breakage was influenced by the type of subgrade. Clearly, ballast degradation was more pronounced for a stiff subgrade (e.g. rock or concrete deck) than that for a relatively soft or weak subgrade. This is in agreement with the laboratory study reported in Section 4.

The ballast breakage index (*BBI*) for Sections B was the least compared to Sections A and C. This finding appears to contradict the general perception that ballast subjected to higher stresses (Section B) would undergo larger deformations due to larger degrees of particle breakage (Lackenby et al. 2007, Nimbalkar et al. 2012). This is because of larger confinement from the barriers of bridge which most likely resulted in a significantly smaller value of BBI. At Sections A and C, however, ballast was allowed to expand more freely in a horizontal direction, thus larger vertical settlement was observed. This observation also confirms that the ability of ballast to expand horizontally also influences the magnitude of track settlement as well as the degree of ballast breakage. These results may also suggest the effectiveness of shock mats in reducing particle degradation when placed above a concrete deck. However, more data from a similar bridge without any shock mat is desirable for more convincing validation.

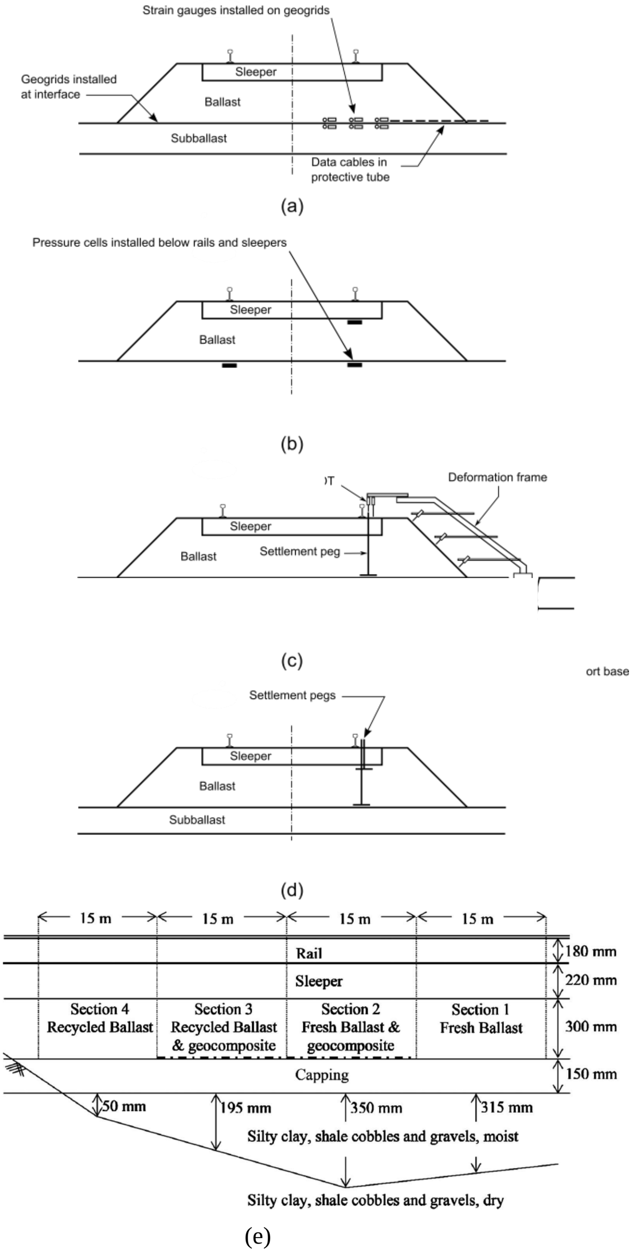

Figure 13 Details of instrumentation of experimental sections of track at Singleton using, (a) strain gauges, (b) pressure cells, (c) deformation frame and (d) settlement pegs; (e) details of track sections

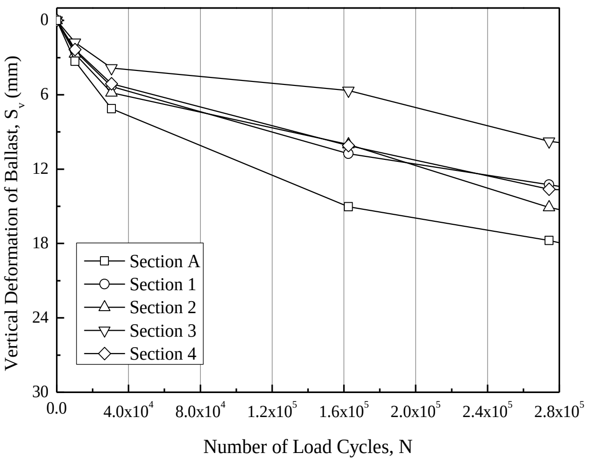

Figure 14 Vertical deformation of ballast layer plotted versus number of load cycles in semi-logarithmic scale for soft embankment (data sourced from Indraratna et al., 2014e)

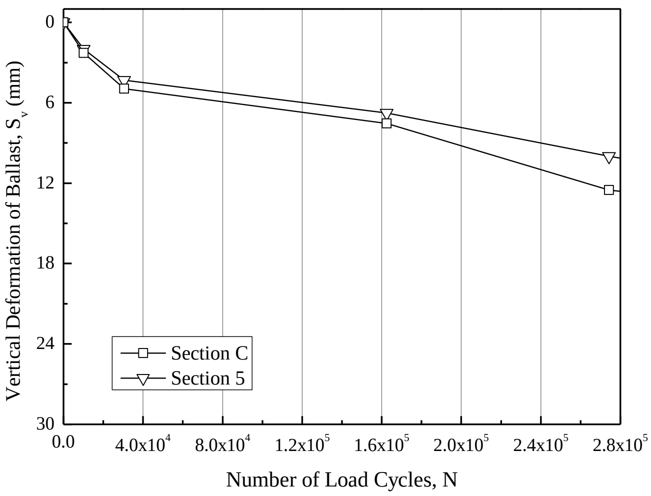

Figure 15 Vertical deformation of ballast layer plotted versus number of load cycles in semi-logarithmic scale for hard rock (data sourced from Indraratna et al., 2014e)

Table 2 Assessment of ballast breakage (data sourced from Indraratna et al. 2014c)

Sr. No.	subgrade	*BBI* top	*BBI* middle	*BBI* bottom
1	alluvial silty clay	0.17	0.08	0.06
2	concrete bridge deck	0.06	0.03	0.02
3	siltstone	0.21	0.11	0.09

7. USE OF SHORT PVDS IN RAILWAY TRACK: FIELD STUDY AT SANDGATE

7.1 Site layout and geology

The Sandgate Rail Grade Separation Project is situated at Sandgate in the Lower Hunter Valley, NSW. Field and laboratory testing was conducted to obtain relevant soil parameters. Site investigation was comprised of 6 boreholes, 14 piezocone tests, 2 in-situ vane shear tests and 2 test pits. Laboratory testing included the determination of soil index properties. Also the standard oedometer and vane shear tests were performed.

The soil profile indicates that the soft compressible formation varies from 4 m to 30 m thick. The lightly overconsolidated soft residual clay is underneath the soft soil layer, which is then followed by a shale stratum. The soil properties are shown in Figure 16, where the groundwater is located at the surface.

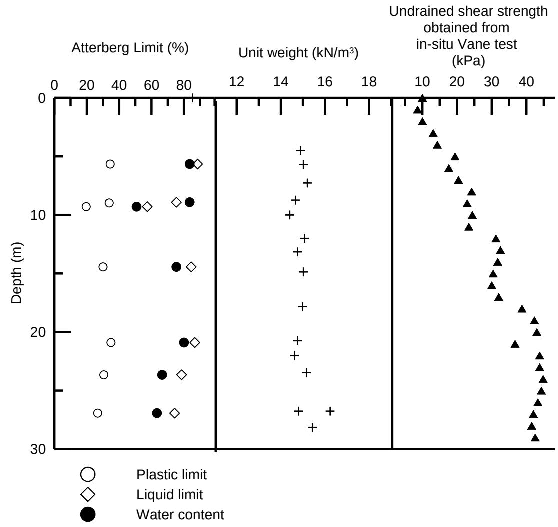

Figure 16 Soil properties at Sandgate Project (Indraratna et al. 2010b)

The moisture contents are similar to their liquid limits. The average soil unit weight was approximately 15 kN/m^3. The undrained shear strength varied between 10 and 40 kPa. The coefficient of consolidation in horizontal direction (c_h) was 2-10 times that in the vertical direction (c_v). Based on preliminary numerical analysis conducted by Indraratna *et al*. (2010b) and Ni *et al.* (2013), short PVDs were suggested and installed at a spacing of 2 m in a triangular pattern up to a depth of 8m. The objectives of the field instrumentations were to: (a) monitor the track stability; (b) assess the performance of the new railway stabilized by PVDs; and (c) investigate the accuracy of the numerical analysis through Class A predictions, where the field monitoring data were unavailable at the time of finite element modeling.

7.2 Finite Element Modeling

Due to time limitation, the rail track was constructed soon after the PVD installation. A train traveling at a very low speed (i.e. 40 km/h) was employed as the only external surcharge. The equivalent dynamic loading considering an impact load factor was adopted for the numerical analysis. A static pressure of 104 kPa with an impact factor of 1.3 was applied according to the relatively low train speed for 25-tonne axle load. The Mohr-Coulomb Model was employed to represent the overconsolidated fill layer, whereas the soft formations were modeled using the Soft Soil Model available in the finite element code, PLAXIS (Brinkgreve 2002). The soil parameters are given elsewhere by Indraratna et al. 2010b and a summary is provided in Table 3.

Table 3 Selected parameters for soft soil layer used in the FEM

Soil layer	*Cohesion C (kPa)*	*Friction angle ϕ (degrees)*	*$\lambda/(1+e_0)$*	*$\kappa/(1+e_0)$*	*pemeability k_h (m/day)*
Soft soil-1	10	25	0.131	0.020	1.4×10^{-4}
Soft soil-2	15	20	0.141	0.017	1.5×10^{-4}

Note: λ *is the virgin compression index of the soil;* κ *is the slope of swelling line*

A mesh discritisation of the formation beneath the rail track is shown in Figure 17. A plane strain finite element analysis based on PLAXIS employed triangular elements with six displacement nodes and three pore pressure nodes. Four rows of PVDs were used in the analysis. An equivalent plane strain analysis with appropriate conversion from axisymmetric to 2D was adopted to analyze the multi-drain analysis (Indraratna et al. 2005b). In this method, the corresponding ratio of the equivalent smear zone permeability to the undisturbed zone permeability for plane strain analysis is:

$$\frac{k_{s,ps}}{k_{h,ps}} = \frac{\beta}{k_{h,ps}/k_{h,ax}\left[\ln(n/s) + k_{h,ax}/k_{s,ax}\ln(s) - 0.75\right] - \alpha} \tag{5}$$

$$\alpha = 0.67(n-s)^3 / n^2(n-1) \tag{5a}$$

$$\beta = 2(s-1)\left[n(n-s-1) + 0.33\left(s^2+s+1\right)\right]/n^2(n-1) \tag{5b}$$

$$n = d_e/d_w \tag{5c}$$

$$s = d_s/d_w \tag{5d}$$

where, d_e = the diameter of the unit cell soil cylinder, d_s = the diameter of the smear zone, d_w= the equivalent diameter of the drain, k_s = horizontal soil permeability in the smear zone, k_h = horizontal soil permeability in the undisturbed zone and the top of the drain and subscripts '*ax*' and '*ps*' denote the axisymmetric and plane strain condition, respectively. The ratio of equivalent plane strain to axisymmetric permeability in undisturbed zone is given by:

$$k_{h,ps}/k_{h,ax} = 0.67(n-1)^2 / \left[n^2\left[\ln(n) - 0.75\right]\right] \tag{6}$$

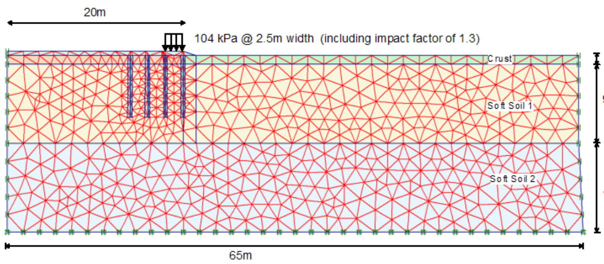

Figure 17 Vertical cross section of rail track and foundation (Indraratna et al. 2010b)

7.3 Comparison of Field Results with Class A FEM Predictions

The field monitoring data were given to the Authors by the track owner (Australian Rail Track Corporation) a year after the FEM analysis. Therefore, all predictions can be classified as *Class A* (Lambe 1973). The calculated and measured vertical settlements at the centre line are shown in Figure 18, which shows that the predicted settlement is in agreement with the field data.

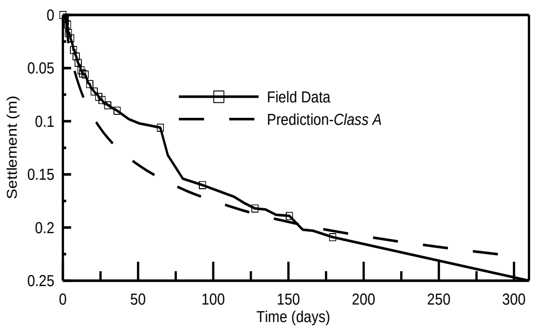

Figure 18 Predicted and measured settlements at the centre line of rail tracks (after Indraratna et al. 2010b)

The *in situ* horizontal displacement at 6 months at the rail embankment toe is presented in Figure 19. As expected, maximum lateral displacements are measured within the upper clay layer (i.e. the softest formation below the 1 m crust) and they are restricted within the topmost compacted crust (depth 0-1 m). The *Class A* predictions of lateral displacements also agree well with the field observations so the effectiveness of PVDs in reducing lateral movement is amply demonstrated in this case study.

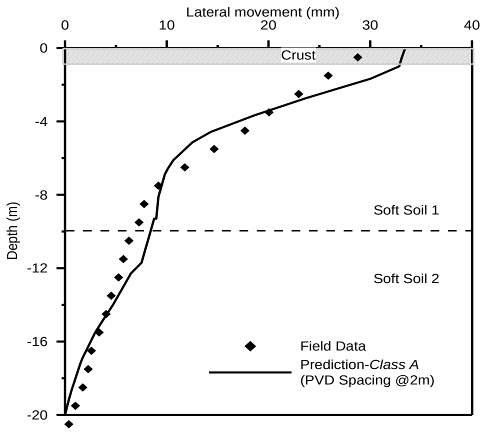

Figure 19 Measured and predicted lateral displacement at the embankment toe at 180 days (after Indraratna et al. 2010b)

8. CONCLUSIONS

This special lecture paper discussed the results of large-scale laboratory tests, numerical modeling using finite element method as well as the findings from full-scale field investigations. The results highlighted that the use of geosynthetics and shock mats have a favourable influence in reducing the deformation of ballast and subgrade.

The large scale triaxial tests revealed that permanent deformation and degradation increased with the frequency and magnitude of load cycles. Three different deformation mechanisms were observed in response to frequency of loading, namely, in Range I: plastic shakedown at $f \leq 20$ Hz, in Range II: plastic shakedown and ratcheting at $30 \text{ Hz} \leq f \leq 50$ Hz, and in Range III: plastic collapse at $f \geq 60$ Hz.

The large-scale impact test results revealed that the shock mats could decrease impact induced strains in ballast by as much as 50%. Impact caused the most significant damage to ballast, especially under high repetitive loads, while just a few impact blows caused considerable ballast damage (i.e. BBI = 17%) when a stiff subgrade was present. However, when a shock mat was placed at the top and bottom of the ballast layer, particle breakage was reduced by approximately 47% over the stiff subgrade.

It was also observed that the optimum geogrid aperture to maximise the interface shear strength was $1.20D_{50}$. In accordance, the effectiveness of different geogrids with nominated aperture sizes were tested under cyclic loading. Lateral Spread Reduction Index (LSRI) was proposed to assess the deformations of geogrid-reinforced ballast. It was shown that LSRI is influenced by the type of geogrid. For geogrids placed at the subballast-ballast interface, LSRI varies from 0.06 to 0.25. However, LSRI increases significantly and attains a maximum value of 0.37 for geogrid placed at 65 mm above the subballast. Both ballast breakage and associated settlements exhibited a significant reduction with the increase in LSRI.

The performance of instrumented ballasted tracks at Singleton was investigated, where different types of geosynthetics and shock mat were installed and monitored. The results of the Singleton study showed that the effectiveness of geogrid increased as the subgrade became weak. The geogrids could decrease the vertical deformations of the ballast, with the obvious benefits of improving track stability and reducing the maintenance cost. Transient deformations of the ballast layer also decreased when geosynthetics were used. The placement of shock mat also helped to mitigate degradation. A *Class A* FEM prediction of the track behavior in comparison with field data proved that short PVDs could increase track stability by significantly decreasing the buildup of excess pore water pressure (PWP) during train passage and being able to facilitate the dissipation of excess PWP during the rest period. In this way, the dissipation of PWP increases track stability for the next loading stage. Both the predictions and field data showed that the lateral displacement can be effectively curtailed by the use of PVDs.

9. ACKNOWLEDGEMENTS

The Authors wish to thank the Australia Research Council, CRC for Rail Innovation, RailCorp (now Sydney Trains), ARTC, ARUP, John Holland, Coffey Geotechnics and Queensland Rail National for their continuous support. The assistance of David Christie (formerly Senior Geotechnical Consultant, Rail Infrastructure Corporation (NSW)) and Tim Neville (ARTC) is gratefully acknowledged. The advice and help over a long period of time by Professor A. Balasubramaniam, Griffith University (Qld) is appreciated. A number of past doctoral students, including Dr Joanne Lackenby, Dr Wadud Salim, Dr Jing Ni and Dr Qideng Sun have all contributed to the contents of this paper. A significant portion of the contents have been reproduced with kind permission from the Journal of Geotechnical and Geoenvironmental Engineering ASCE, Proceedings of the Institution of Civil Engineers – Ground Improvement and Canadian Geotechnical Journal.

10. REFERENCES

Auersch, L. (2006). Dynamic axle loads on tracks with and without ballast mats: numerical results of three-dimensional vehicle-track-soil models. Proc., Inst. Mech. Eng. Part F, 220(2), 169-183.

Bergado, D. T., Balasubramaniam, A. S., Fannin, R. J., and Holtz, R. D. (2002). Prefabricated vertical drains (PVDs) in soft Bangkok clay: a case study of the new Bangkok International Airport Project, Can. Geotech. J., 39, pp304-315.

Bian, J., Gu, Y., and Murray, M. H. (2013) "A dynamic wheel–rail impact analysis of railway track under wheel flat by FE analysis", Vehicle System Dynamics, 51, Issue 6, pp784-797.

Brinkgreve, R.B.J. (2002) PLAXIS (Version 8) User's Manual. Delft University of Technology PLAXIS B.V., Netherlands.

Brown, S. F., Kwan, J., and Thom, N. H. (2007) "Identifying the key parameters that influence geogrid reinforcement of railway ballast", Geotext. Geomembr., 25, Issue 6,pp326-335.

Frederick, C. O. and D. J. Round. Vertical Track Loading, Track Technology, Thomas Telford Ltd, 1985, London.

Indraratna B., and Redana I. W. (2000) "Numerical modeling of vertical drains with smear and well resistance installed in soft clay", Can. Geotech. J., 37, Issue 1, pp133-145.

Indraratna B., and Salim W. (2003) "Deformation and degradation mechanics of recycled ballast- stabilised with geosynthetics". Soils and Foundations, 43, Issue 4, pp35-46

Indraratna, B., Lackenby, J. and Christie, D. (2005a) "Effect of confining pressure on the degradation of ballast under cyclic loading", Géotechnique, 55, Issue 4, pp325-328.

Indraratna, B., Rujikiatkamjorn C., and Sathananthan, I. (2005b) "Analytical and numerical solutions for a single vertical drain including the effects of vacuum preloading", Can. Geotech. J., 42, Issue 4, pp994-1014.

Indraratna B., Shahin, M. A., and Salim, W. (2007) "Stabilisation of granular media and formation soil using geosynthetics with special reference to railway engineering", Ground Improvement, 11, Issue 1, pp27-43.

Indraratna, B., Aljorany, A., and Rujikiatkamjorn C., (2008) "Analytical and numerical modelling of consolidation by sand drains beneath a circular embankment", International Journal of Geomechanics, ASCE, 8, Issue 3, pp199-206.

Indraratna, B., Attya, A., and Rujikiatkamjorn, C. (2009) "Experimental investigation on effectiveness of a vertical drain under cyclic loads", J. Geotech. Geoenviron. Eng., 135, Issue 6, pp835-839.

Indraratna B., Nimbalkar S., Christie D., Rujikiatkamjorn C., and Vinod J. S. (2010a) "Field Assessment of the Performance of a Ballasted Rail Track with and without Geosynthetics", J. Geotech. Geoenviron. Eng., 136, Issue 7, pp907-917.

Indraratna, B., Rujikiatkamjorn, C., Ewers, B., and Adams, M. (2010b) "Class A prediction of the behaviour of soft estuarine soil foundation stabilised by short vertical drains beneath a rail track", J. Geotech. Geoenviron. Eng. 136, Issue 5, pp686-696.

Indraratna, B., Rujikiatkamjorn, C., Ameratunga, J., and Boyle, P. (2011) "Performance and prediction of Vacuum Combined Surcharge Consolidation at Port of Brisbane", J. Geotech. Geoenviron. Eng, ASCE, 137, Issue 11, pp1009-1018.

Indraratna, B., Rujikiatkamjorn, C., Balasubramaniam, A. S., and McIntosh, G. (2012a) "Soft ground improvement via vertical drains and vacuum assisted preloading", Geotextiles and Geomembranes, 30, Issue 1, pp16-23.

Indraratna, B., Tennakoon, N., Nimbalkar, S. and Rujikiatkamjorn, C. (2012b). Behaviour of Clay Fouled Ballast under Drained Triaxial Testing. Géotechnique, 63(5); 410-419.

Indraratna, B., Nimbalkar, S., and Neville, T. (2013a) "Performance assessment of reinforced ballasted rail track", Ground Improvement, 167, Issue 1, pp24-34.

Indraratna, B., and Nimbalkar, S. (2013) "Stress-strain degradation response of railway ballast stabilized with geosynthetics", J. Geotech. Geoenviron. Eng., 139, Issue 5, pp684-700.

Indraratna, B., Hussaini, S. K. K., and Vinod, J. S. (2013b) "The lateral displacement response of geogrid-reinforced ballast under cyclic loading", Geotext. Geomembr., 39, pp20-29.

Indraratna, B., Nimbalkar, S., Coop, M., and Sloan, S.W. (2014a) "A constitutive model for coal-fouled ballast capturing the effects of particle degradation", Computers and Geotechnics, 61, Issue 9, pp96-107.

Indraratna, B., Sun, Q. D., and Nimbalkar, S. (2014b) "Observed and predicted behaviour of rail ballast under monotonic loading capturing particle breakage", Can. Geotech. J., 52, Issue 1, pp73-86.

Indraratna, B., Nimbalkar, S. S., and Rujikiatkamjorn, C. (2014c) "Enhancement of rail track performance through utilisation of geosynthetic inclusions", Geotechnical Engineering Journal of the SEAGS & AGSSEA, 45, Issue 1, pp17-27.

Indraratna, B., Nimbalkar, S., Navaratnarajah, S. K., Rujikiatkamjorn, C., and Neville, T. (2014d) "Use of shock mats for mitigating degradation of railroad ballast", Sri Lankan Geotechnical Society Journal 6, Issue 1, pp 32-41.

Indraratna, B., Nimbalkar, S., and Rujikiatkamjorn, C. (2014e) "From theory to practice in track geomechanics - Australian perspective for synthetic inclusions", Transportation Geotechnics Journal, 1, Issue 4, pp171-187.

Indraratna, B., Biabani, M., and Nimbalkar, S. (2015) "Behavior of geocell-reinforced subballast subjected to cyclic loading in plane-strain condition", J. Geotech. Geoenviron. Eng., 141, Issue 1, 04014081.

Jenkins, H. M., Stephenson, J. E., Clayton, G. A., Moorland, J. W., and Lyon, D. (1974) "The effect of track and vehicle parameters on wheel/rail vertical dynamic forces", Railway Engineering Journal, 3, Issue 1, pp2-16.

Kaewunruen, S., and Remennikov, A. (2010) "Dynamic crack propagations in prestressed concrete sleepers in railway Track systems subjected to severe impact loads", Journal of Structural Engineering, 136, Issue 6, pp749-754.

Lackenby, J., Indraratna, B., and McDowell, G. (2007) "Effect of confining pressure on ballast degradation & deformation under cyclic loading", Geotechnique, 57, Issue 6, pp527-536.

Lambe, T. W. (1973) "Predictions in soil engineering", Geotechnique, 23, Issue 2, pp149-202.

Li, D., and Davis, D. (2005) "Transition of Railroad Bridge Approaches", Journal of Geotechnical and Geoenvironmental Engineering ASCE, 131, Issue 11, pp1392-1398.

Ni, J., Indraratna, B., Geng, X. Y. Carter, J. P., and Rujikiatkamjorn C. (2013) "Radial consolidation of soft soil under cyclic loads", Computers and Geotechnics, 50, Issue 1, pp1-5.

Ngo, N. T., Indraratna, B., and Rujikiatkamjorn, C., (2014). DEM simulation of the behaviour of geogrid stabilised ballast fouled with coal. Computers and Geotechnics, 55, 224–231.

Nimbalkar, S., Indraratna, B., Dash, S., and Christie, D. (2012) "Improved performance of railway ballast under impact loads using shock mats", J. Geotech. Geoenviron. Eng., 138, Issue 3, pp281-294.

Raymond, G. P. (2002) "Reinforced ballast behaviour subjected to repeated load", Geotext. Geomembr. 20, Issue 1, pp39-61.

Selig, E. T., and Waters, J. M. (1994). Track Geotechnology and Substructure Management, Thomas Telford, London. Standards Australia (1996), Aggregates and rock for engineering purposes Part 7: Railway ballast, AS 2758.7-1996, Australia.

Steffens, D., and Murray, M. (2005) "Establishing meaningful results from models of railway track dynamic behaviour", Proceedings of 8th IHHA Conference, Brazil, pp41-50.

Sun, Q. D., Indraratna, B., and Nimbalkar, S. (2014). "Effect of cyclic loading frequency on the permanent deformation & degradation of railway ballast", Géotechnique, 64, Issue 9, pp746-751.

Sun, Q. D., Indraratna, B., and Nimbalkar, S. (2015). "The deformation and degradation mechanisms of railway ballast under high frequency cyclic loading", J. Geotech. Geoenviron. Eng., 10.1061/(ASCE)GT.1943-5606.0001375.

Tennakoon, N., Indraratna, B., Nimbalkar, S., and Sloan, S.W. (2015) "Application of bounding surface plasticity concept for clay-fouled ballast under drained loading", Computers and Geotechnics, 70, Issue 10, pp96-105.